

## THE INTERSTELLAR MEDIUM AROUND THE SUPERNOVA REMNANT G320.4–1.2

G. M. DUBNER,<sup>1,2</sup> B. M. GAENSLER,<sup>3,4,5</sup> E. B. GIACANI,<sup>1,2</sup> W. M. GOSS,<sup>6</sup> AND A. J. GREEN<sup>7</sup>

Received 2001 August 9; accepted 2001 October 10

### ABSTRACT

Using the Australia Telescope Compact Array, we have carried out a survey of the H I emission in the direction of the barrel-shaped supernova remnant (SNR) G320.4–1.2 (MSH 15-52) and its associated young pulsar B1509–58. The angular resolution of the data is  $4'0 \times 2'7$ , and the rms noise is of order 30 mJy beam<sup>-1</sup> ( $\sim 0.5$  K). The H I observations indicate that the north-northwest radio limb has encountered a dense H I filament (density  $\sim 12$  cm<sup>-3</sup>) at the same LSR velocity as that of the SNR ( $V_{\text{LSR}} \sim -68$  km s<sup>-1</sup>). This H I concentration would be responsible for the flattened shape of the northwestern lobe of G320.4–1.2 and for the formation of the radio-optical–X-ray nebula RCW 89. The emission associated with the bright knots in the interior of RCW 89 can be explained as arising from the interaction between the collimated relativistic outflow from the pulsar and the denser part of this H I filament (density  $\sim 15$  cm<sup>-3</sup>). The south-southeastern half of the SNR, on the other hand, seems to have rapidly expanded across a lower density environment (density  $\sim 0.4$  cm<sup>-3</sup>). The H I data also reveal an unusual H I feature aligned with a collimated outflow generated by the pulsar, suggestive of association with the SNR. The anomalous kinematical velocity of this feature ( $V_{\text{LSR}} \sim 15$  km s<sup>-1</sup>), however, is difficult to explain.

*Key words:* ISM: individual (G320.4–1.2, RCW 89) — ISM: structure — pulsars: individual (B1509–58) — supernova remnants

### 1. INTRODUCTION

The radio morphologies of supernova remnants (SNRs) are usually approximated by limb-brightened spherical shells, in which the shock front accelerates electrons to synchrotron radiation-emitting energies. However, observations at increasingly higher resolution and sensitivity have demonstrated that actual SNR morphologies are much more complex, exhibiting breakout, barrel, and helical patterns<sup>8</sup> (Manchester 1987; Dubner et al. 1996, 1998b; Whiteoak & Green 1996; Gaensler 1998). Such a diversity reflects not only variations in the properties of the progenitor star and of the explosion itself but also echoes the physical conditions of circumstellar and interstellar gas and magnetic fields. The interpretation of SNR morphologies has the additional complication that the images observed are a two-dimensional projection of a three-dimensional object. Radio spectroscopy of the interstellar medium (ISM) provides a valuable tool to unravel these three-dimensional effects by using kinematic signatures. As part of an ongoing effort to study the interaction of SNRs with their environment (Dubner et al. 1998a, 1998b, 1999; Giacani et al. 2000), we present a study of the distribution and kinematics of the neutral hydrogen in the vicinity of SNR G320.4–1.2 (MSH 15-52).

SNR G320.4–1.2 has an unusual radio morphology consisting of two loosely connected emission regions, one to the northwest and the other to the south-southeast. Figure 1 shows the radio and X-ray emission from the SNR. The young pulsar PSR B1509–58 lies between the two main radio components of the SNR; the pulsar's position as measured by Gaensler et al. (1999), hereafter G99, is marked in Figure 1 with a cross. The optical-radio–X-ray nebula RCW 89 is located on the northwestern extreme of G320.4–1.2.

Like many other SNRs, G320.4–1.2 has a bilateral or barrel morphology (Kesteven & Caswell 1987; Gaensler 1998). Many different mechanisms have been proposed to account for this morphology, relating both to the progenitor star and supernova explosion (intrinsic effects; Kesteven & Caswell 1987; Manchester 1987; Brighenti & D'Ercole 1994; Willingale et al. 1996) and to subsequent interaction with the SNR environment (extrinsic effects; Bisnovatyi-Kogan, Lozinskaya, & Silich 1990; Fulbright & Reynolds 1990). Most recently, Gaensler (1998) has argued that the bilateral appearance arises when an SNR expands into an elongated low-density cavity; the radio emission then originates at the sites where the shock encounters the walls of the cavity.

This peculiar SNR and its energetic young pulsar have been extensively observed throughout the electromagnetic spectrum (see G99 for a summary of previous observations). In particular, recent X-ray and radio data provide convincing evidence that the SNR and pulsar resulted from a single supernova explosion, which occurred approximately 1700 years ago (Tamura et al. 1996; Brazier & Becker 1997; G99; Gaensler et al. 2001). Specifically, G99 argue that the entire complex can be interpreted as the result of a low-mass or high-energy explosion occurring near one edge of an elongated low-density ( $n \sim 0.01$  cm<sup>-3</sup>) cavity. To the northwest the SNR has expanded into dense material ( $n \sim 1\text{--}5$  cm<sup>-3</sup>), while to the southeast the remnant has expanded rapidly across the low-density cavity. Meanwhile, the pulsar

<sup>1</sup> Instituto de Astronomía y Física del Espacio (CONICET, UBA), C.C. 67, 1428 Buenos Aires, Argentina; gdubner@iafe.uba.ar.

<sup>2</sup> Member of the Carrera del Investigador Científico of CONICET, Argentina.

<sup>3</sup> Center for Space Research, Massachusetts Institute of Technology, 70 Vassar Street, Cambridge, MA 02139.

<sup>4</sup> Hubble Fellow.

<sup>5</sup> Current address: Harvard-Smithsonian Center for Astrophysics, 60 Garden Street, Cambridge, MA 02138.

<sup>6</sup> National Radio Astronomy Observatory, P.O. Box O, Socorro, NM 87801.

<sup>7</sup> School of Physics, University of Sydney, A28, NSW 2006, Australia.

<sup>8</sup> See <http://www.physics.usyd.edu.au/astrop/wg96cat/>.

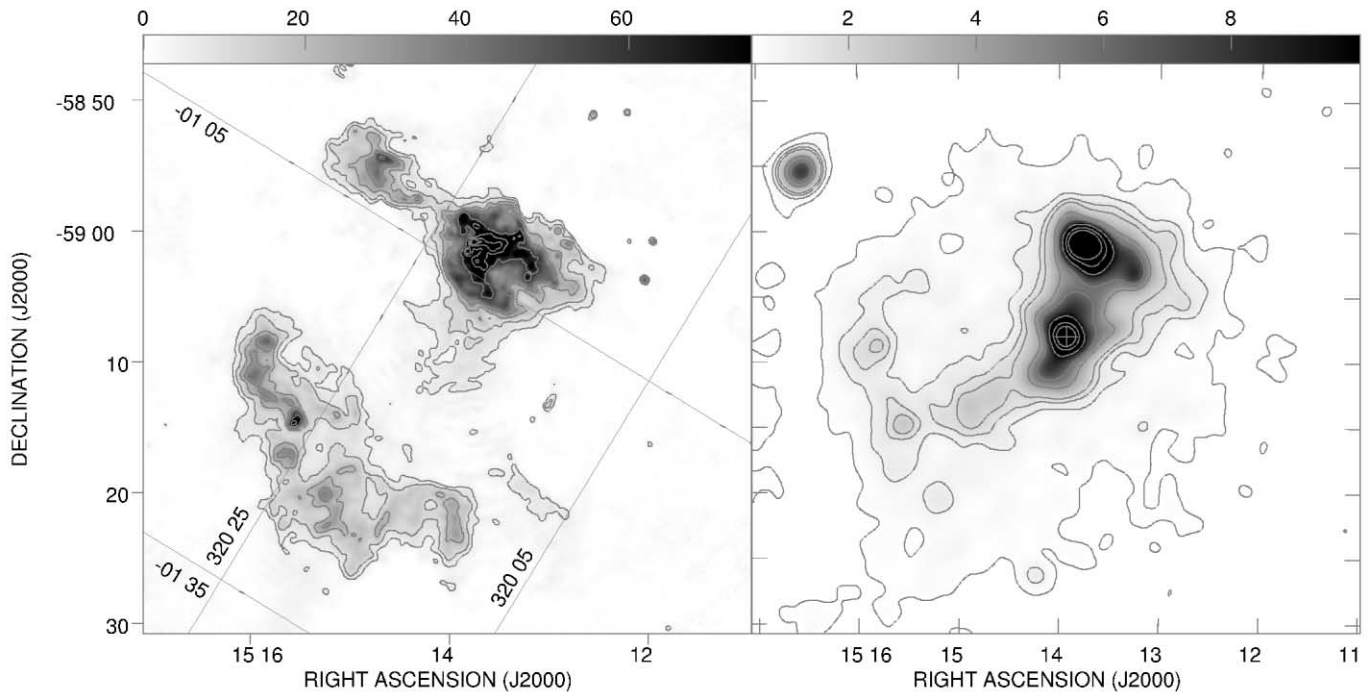


FIG. 1.—*Left*: Radio continuum image of the SNR G320.4–1.2 at 1.4 GHz, at a resolution of  $24'' \times 21''$  (G99). The gray scale varies linearly from 0 to  $+75 \text{ mJy beam}^{-1}$ , while contours are at levels of 5, 10, 20, 30, 60, 90, 120, and  $150 \text{ mJy beam}^{-1}$ . A few Galactic coordinate lines are included for reference. *Right*: Gray-scale and contour *ROSAT* PSPC X-ray image of G320.4–1.2 (Trussoni et al. 1996). The contour levels (in arbitrary units) are 0.5, 1, 1.5, 2, 4, 6, 10, 15, and 20. The white cross indicates the position of PSR B1509–58 as determined from interferometric measurements (G99).

appears to be generating twin collimated outflows, the northern of which is interacting with the SNR to produce a collection of compact radio–X-ray knots embedded in RCW 89. A distance of  $5.2 \pm 1.4 \text{ kpc}$  was derived for G320.4–1.2 by G99, based on H I absorption measurements, in agreement with the results of Caswell et al. (1975).

Within this complex scenario, it is clear that the interpretation of the existing body of observational data can greatly benefit from an accurate knowledge of the distribution and kinematics of the surrounding neutral hydrogen emission. Here we report on an H I survey of SNR G320.4–1.2 and its environment, carried out with the Australia Telescope Compact Array.

## 2. OBSERVATIONS AND DATA REDUCTION

Interferometric H I observations toward G320.4–1.2 were carried out using the Australia Telescope Compact Array (ATCA; Frater, Brooks, & Whiteoak 1992), a six-element synthesis telescope located near Narrabri, NSW, Australia, during a session of 13 hr on 1998 October 13. To achieve optimal  $u-v$  coverage in the radial direction, the array was used in the nonstandard 210 m configuration, in which five antennas are positioned closely together to provide 10 baselines ranging from 31 to 214 m. The sixth (fixed) antenna is separated from the other five elements by 5–6 km, and was not used in our analysis.

A region surrounding the SNR was surveyed in a mosaic of 19 pointings, following a hexagonal grid to cover  $6 \text{ deg}^2$ . The separation between grid points of about  $16'$  satisfies the Nyquist sampling criterion for the primary beam width of  $33'$  (FWHM). Observations were centered at a frequency of 1420 MHz, using 1024 channels over a total bandwidth of 4

MHz. The absolute flux density scale was determined by assuming a flux density for PKS B1934–638 of  $14.85 \text{ Jy}$  at 1.42 GHz. Observations of PKS B1934–638 were also used to determine the spectral response across the observing band. Time variability in the antenna gains was calibrated using regular observations of PKS B1540–828. After editing and calibration, continuum emission was subtracted from the data in the  $u-v$  plane using the task UVLSF in AIPS (van Langevelde & Cotton 1990). The data were then transferred to the MIRIAD package<sup>9</sup> (Sault & Killeen 1999), where all pointings were imaged simultaneously to form 390 mosaicked planes, covering LSR velocities between  $-150$  and  $+171 \text{ km s}^{-1}$  at a velocity resolution of  $1 \text{ km s}^{-1}$  (channel separation of  $0.82 \text{ km s}^{-1}$ ). This cube was then deconvolved using a mosaicked maximum entropy technique (Sault, Staveley-Smith, & Brouw 1996) and then convolved with a Gaussian restoring beam.

Any analysis of H I emission requires measurements at all spatial scales down to the resolution limit. However, our ATCA observations are not sensitive to structures larger than  $15'–20'$ . To recover this short-spacing data, we have utilized H I observations made using the Parkes 64 m radio telescope, carried out as part of the Southern Galactic Plane Survey (SGPS; McClure-Griffiths et al. 2001) with an angular resolution of  $14'$ . The Parkes data were multiplied by a factor of 0.9 to match the flux calibration applied to the ATCA data; interferometric and single-dish data were then appropriately weighted according to their respective primary beam shapes and combined using the task IMMERGE in MIRIAD<sup>9</sup> (Stanimirović 1999; Sault & Killeen 1999). The units of the final combined cube are janskys

<sup>9</sup> See <http://www.atnf.csiro.au/computing/software/miriad/>.

per beam. To convert to units of brightness temperature, these data must be multiplied by a factor of  $16.3 \text{ K Jy}^{-1}$  beam. The angular resolution of the data is  $4'.0 \times 2'.7$  (position angle  $55^\circ$ ), and the rms in line-free channels is  $\sim 30 \text{ mJy beam}^{-1}$  ( $\sim 0.5 \text{ K}$ ).

### 3. RESULTS

#### 3.1. General H I Distribution

Figure 2 illustrates the general properties of H I emission in the direction of G320.4–1.2. The top shows an average H I profile of the observed region taken from the Parkes SGPS data, while the bottom displays the circular rotation model toward ( $l = 320^\circ$ ,  $b = -1^\circ$ ), assuming  $R_0 = 8.5 \text{ kpc}$  and  $\Theta_0 = 220 \text{ km s}^{-1}$  and using the rotation curve of Fich, Blitz & Stark (1989).

The neutral hydrogen emission in this direction has a complex structure and is spread over more than  $200 \text{ km s}^{-1}$ . The five main peaks of this spectrum can be interpreted as emission from gas related to the Sagittarius-Carina galactic arm (which the line of sight crosses at both  $V_{\text{LSR}} \sim -50$  and

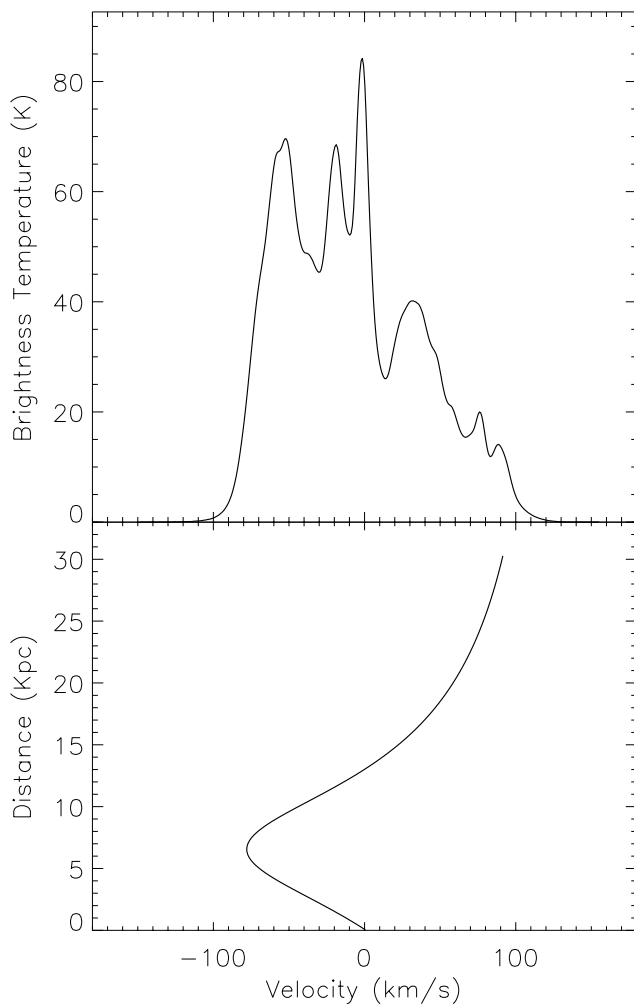


FIG. 2.—*Top*, Average profile of the H I emission as taken from Parkes measurements toward the SNR G320.4–1.2, obtained as part of the Southern Galactic Plane Survey; *bottom*, Galactic rotation curve for  $l = 320^\circ$ ,  $b = -1^\circ$ , according to the Galactic circular rotation model of Fich, Blitz, & Stark (1989).

about  $+80 \text{ km s}^{-1}$ ), to the Scutum-Crux arm (at velocities of  $V_{\text{LSR}} \sim -20$  and  $+40 \text{ km s}^{-1}$ ), and to the local gas contribution near  $0 \text{ km s}^{-1}$ . The SNR would be located on the far border of the Carina arm (Georgelin et al. 1987).

We investigate the H I emission distribution in the entire observed velocity interval, looking for morphological and/or kinematical evidence of interaction of G320.4–1.2 and its different components with the surrounding H I gas. Figure 3 provides an overview of the distribution of atomic hydrogen in the surveyed region. It displays the H I emission between about  $-81$  and about  $+92 \text{ km s}^{-1}$ , the interval in which significant H I emission is found. Each image is the average of six consecutive spectral channels, spanning  $5 \text{ km s}^{-1}$ ; however, the analysis is carried out with the highest possible velocity resolution. The field shown is slightly reduced in size with respect to the observed field to avoid edge effects. The velocity shown at lower left of each image corresponds to the velocity of the first integrated channel. Superposed on the H I images are a few representative contours of the radio continuum emission of G320.4–1.2 at  $1.4 \text{ GHz}$  as taken from G99, at a spatial resolution of  $24'' \times 21''$ .

From about  $-76$  to about  $-66 \text{ km s}^{-1}$ , the most conspicuous feature in H I is an elongated filament seen partially overlapping the bright northwestern part of the SNR. This filament runs diagonally from northwest to southeast, in a direction parallel to the Galactic plane. This filament is discussed in detail in the next section.

From  $\sim 60$  to  $\sim 40 \text{ km s}^{-1}$ , a strong gradient in the gas density (assumed to be optically thin) between the northwestern half of the field (closer to the Galactic plane) and the southeastern corner (away from the Galactic plane) is evident. This density gradient persists up to  $V \sim -31 \text{ km s}^{-1}$ , although with less contrast than at more negative velocities. Significant absorption is evident against bright continuum emission from RCW 89 in this velocity range. (See also G99.)

From about  $-26$  to  $\sim 0 \text{ km s}^{-1}$ , the H I emission appears quite uniformly distributed, with a few brighter concentrations near the northwestern corner. Strong absorption against RCW 89 is observed at these velocities. In the most severe cases, this absorption is surrounded by residual sidelobes, which were not completely removed in the deconvolution process.

Positive velocities along this line of sight correspond to distant gas, located beyond  $\sim 12 \text{ kpc}$  (see Fig. 2). We have examined the H I emission at positive velocities, bearing in mind that these data can also include contributions from closer gas, which might be associated with G320.4–1.2 but which has been kinematically disturbed.

In the velocity range between  $-1.5$  and  $8 \text{ km s}^{-1}$  (i.e., in the images labeled  $-1.5$  and  $+3.5 \text{ km s}^{-1}$  in Fig. 3), two parallel bands of H I emission cross over the field from northeast to southwest. The H I concentration that runs close to the southeastern lobe of G320.4–1.2 shows good morphological correspondence with the radio continuum emission of the SNR. This H I filament, as seen in projection, surrounds the southeastern lobe of the SNR along the eastern and southern borders. Such correspondence is even closer when comparing the H I distribution with the X-ray emission. However, since at this kinematical velocity there is no way to disentangle the contribution of gas likely to be associated with G320.4–1.2 from the intense local gas emission, we do not consider this structure a firm candidate for H I–SNR association.

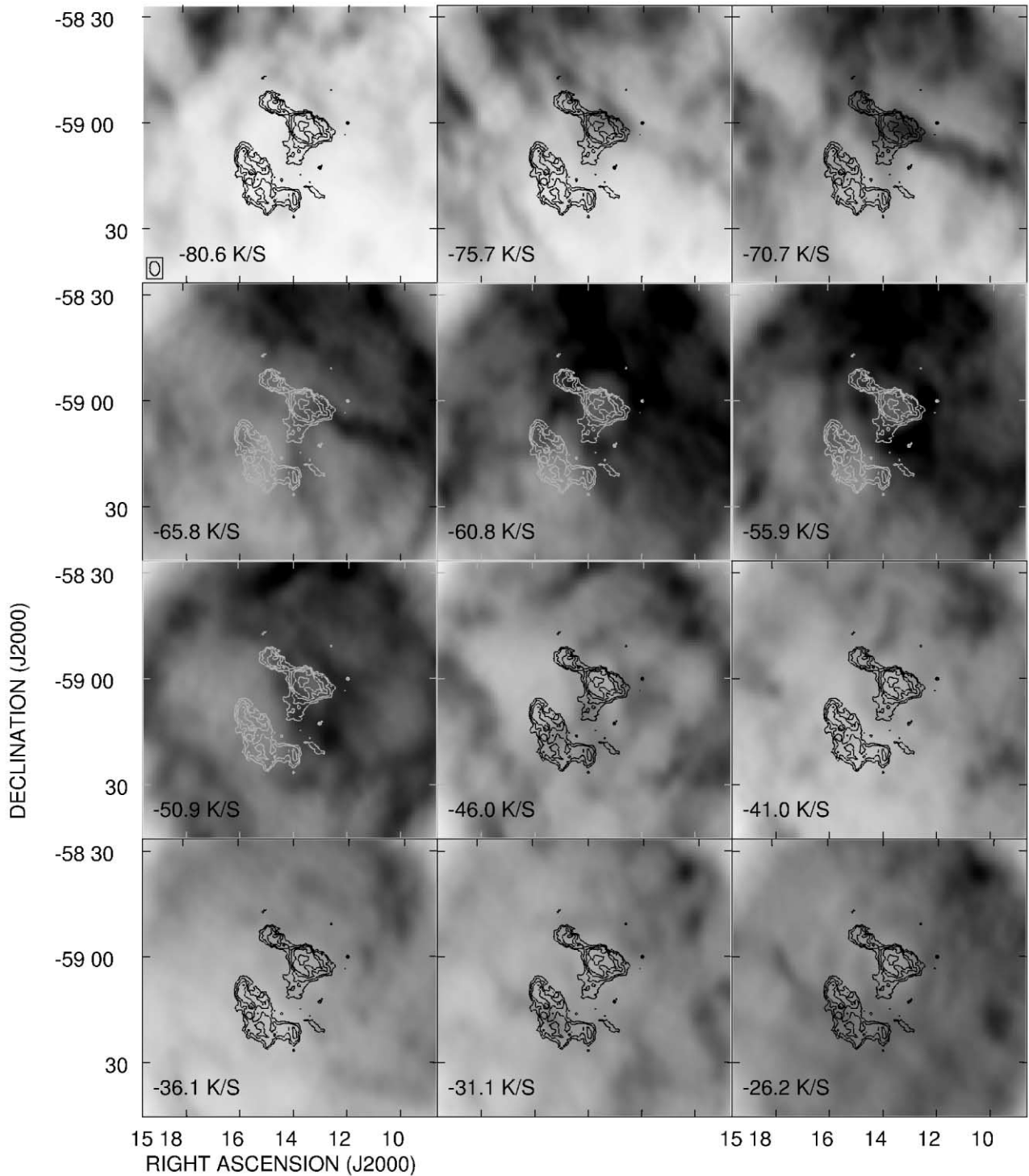


FIG. 3.—Images of the H I emission between LSR velocities of about  $-81$  and about  $+92$   $\text{km s}^{-1}$ , each integrated over six consecutive channels (approximately  $5$   $\text{km s}^{-1}$ ). The velocity shown at lower left in each image corresponds to the first integrated channel; the gray scale for the images varies between  $+0.08$  and  $+6$   $\text{Jy beam}^{-1} \text{km s}^{-1}$ . The resolution of the data is  $4'.0 \times 2'.7$  at position angle  $55^\circ$  (measured north through east). Superposed on the H I images are a few representative contours of the radio continuum emission of G320.4–1.2 at  $1.4$  GHz (G99).

From  $\sim 13$  to  $\sim 22$   $\text{km s}^{-1}$ , there is an unusual bright filament oriented almost perpendicular to the Galactic plane, breaking the plane-parallel symmetry observed otherwise. This filament overlaps both the brightest region of the SNR and the pulsar itself, and will be discussed further in the next section.

At  $+33$  and  $+38$   $\text{km s}^{-1}$  a long, moderately bright H I filament is observed in apparent contact with the northwestern

half of the SNR. However, since most of the H I in this direction is expected to have this plane-parallel distribution, we conclude that this feature is most probably distant background material, located  $14$  kpc away. The remaining high-velocity images show no features that can be feasibly associated with G320.4–1.2.

To determine the systemic velocity of G320.4–1.2, we can use Figure 3 to analyze the characteristics of the H I near

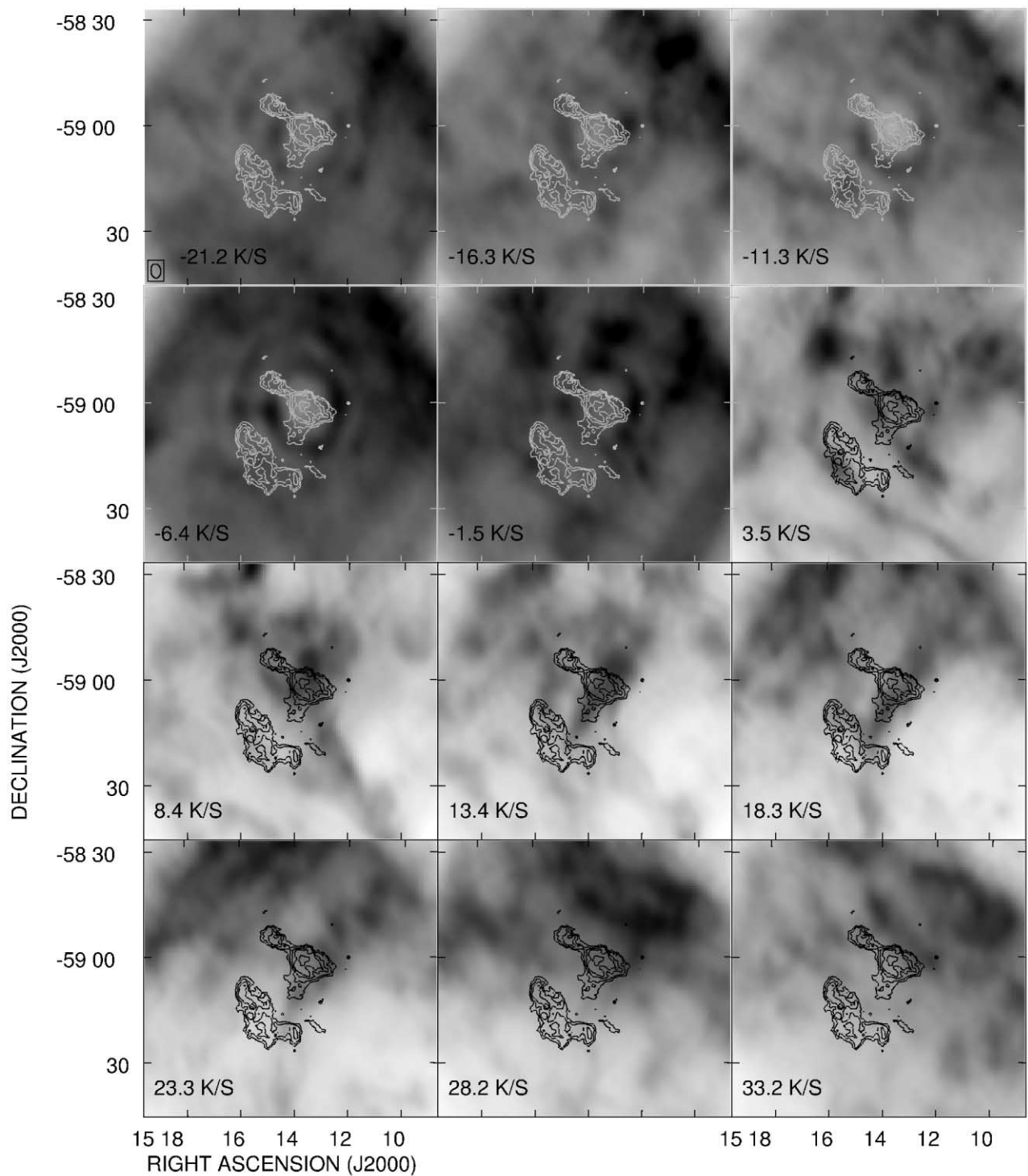


FIG. 3.—Continued

the SNR. In agreement with previous H I absorption studies (Caswell et al. 1975, G99), the images in Figure 3 show that H I absorption is present toward RCW 89 in the velocity range between  $-61$  and  $-51$   $\text{km s}^{-1}$ . Thus, the kinematical velocity corresponding to G320.4–1.2 must be more negative than  $-61$   $\text{km s}^{-1}$ . In addition, H I is observed in emission near the northern portion of the remnant up to  $V_{\text{LSR}} \simeq -76$   $\text{km s}^{-1}$ . We therefore conclude that the systemic velocity of G320.4–1.2 lies in the range  $-76$  to  $-61$   $\text{km s}^{-1}$ . Adopting a systemic velocity of  $V_{\text{LSR}} \sim -68$   $\text{km}$

$\text{s}^{-1}$ , the kinematical distance to the source turns out to be about 5 kpc, in good agreement with a previous estimate by G99.

### 3.2. Particular H I Features

In this section we focus on specific H I features, searching for favorable H I–SNR associations.

1. *The northern filament in the interval  $-76 \lesssim V_{\text{LSR}} \lesssim -66$   $\text{km s}^{-1}$ .*—This velocity interval corre-

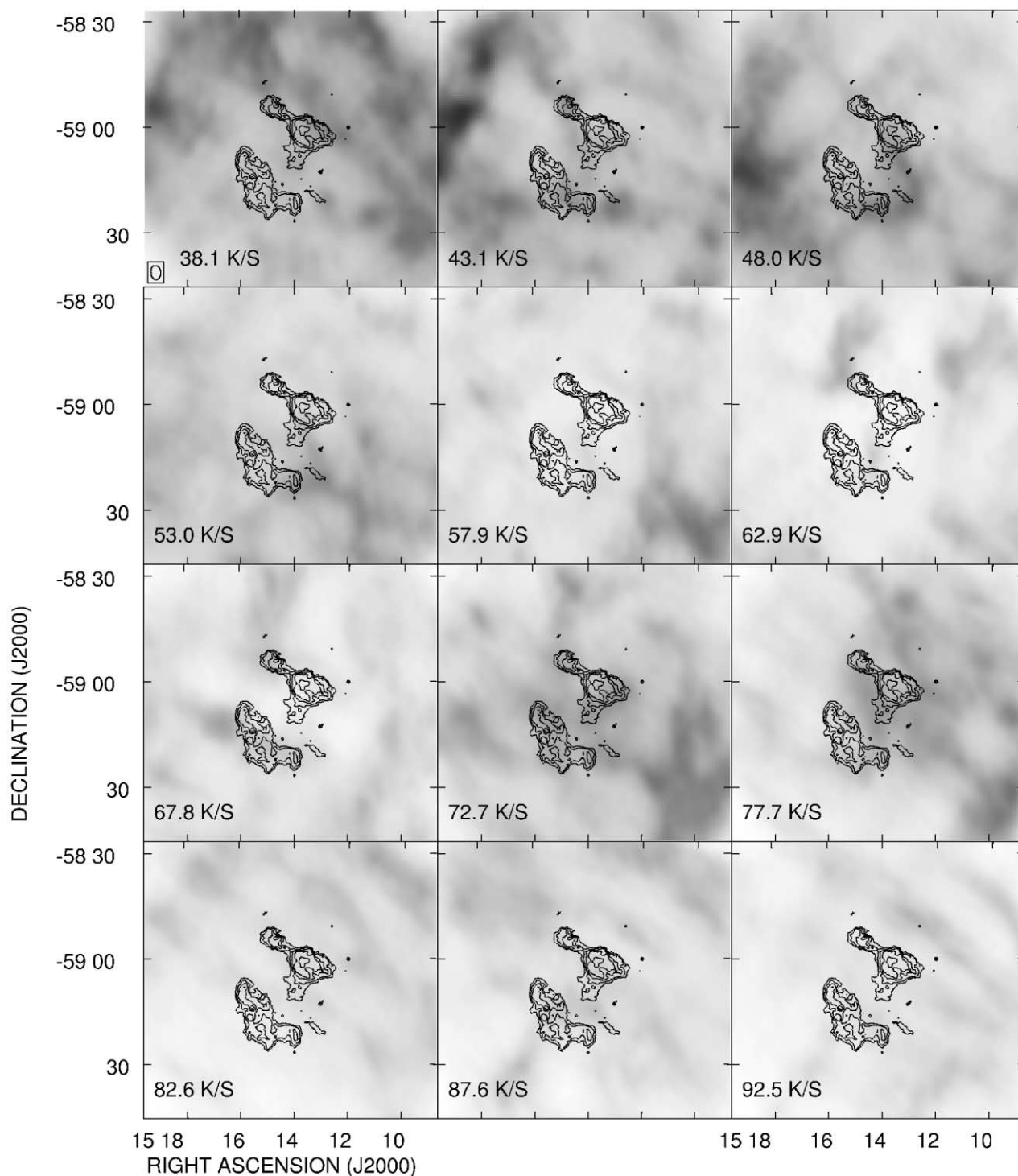


FIG. 3.—Continued

sponds to the systemic velocity of G320.4–1.2. Figure 4 shows in gray scale the H I distribution obtained by integrating between velocities of  $-76$  and  $-66$   $\text{km s}^{-1}$ . The 1.4 GHz radio continuum emission from G320.4–1.2 (as taken from G99) is plotted in contours. This extended H I filament to the northwest may represent the dense external wall previously suggested by G99 to be slowing down the expansion of G320.4–1.2 in this direction. This feature may also be responsible for the flattened shape of the northwestern lobe

of the bilateral SNR. In particular this filament has a peak in H I emission (brightness temperature  $80$  K at  $v = 70$   $\text{km s}^{-1}$ ) exactly overlapping RCW 89. We propose that this H I cloud (about  $7'$  in diameter), associated with RCW 89, is the dense material with which the SNR has collided and with which the outflow from the pulsar is interacting (Tamura et al. 1996; G99). According to this interpretation, the bright nebula RCW 89 (or, more precisely, the bright radio–X-ray knots in its interior) has formed at the site of interaction

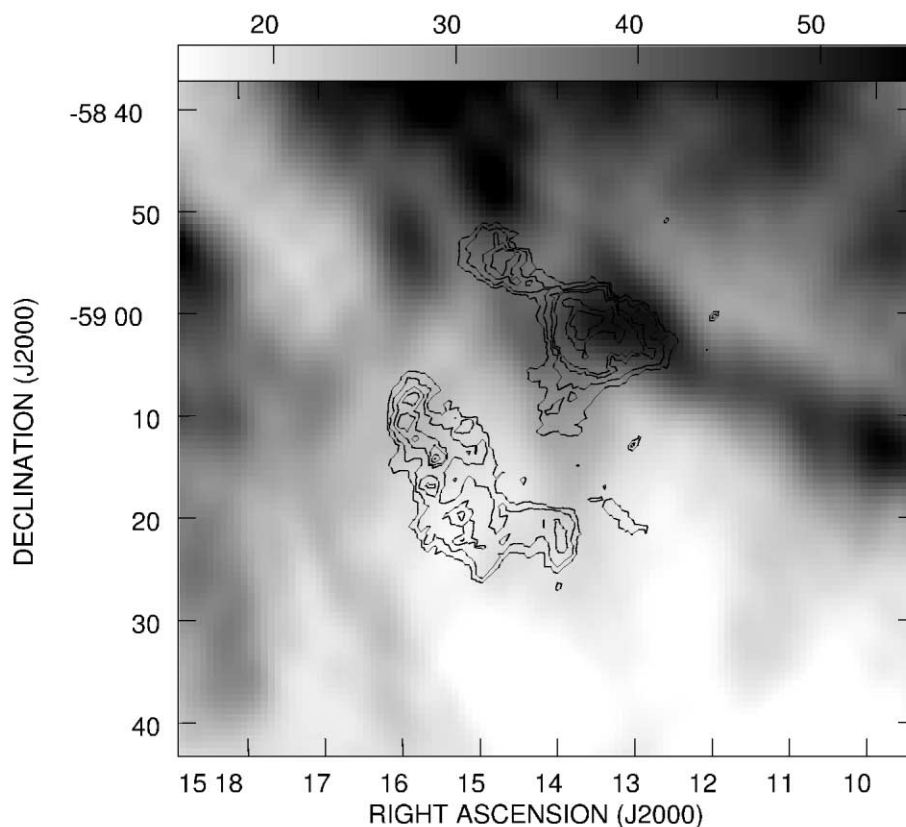


FIG. 4.—Comparison between radio continuum and H I in the velocity range  $-76$  to  $-66$   $\text{km s}^{-1}$ . The gray scale, ranging from 15 to 55  $\text{mJy beam}^{-1} \text{ km s}^{-1}$ , corresponds to the H I distribution, while the contours represent the radio continuum emission at 1.4 GHz (G99.) Plotted contours are 5, 10, 20, 30, 60, and 90  $\text{mJy beam}^{-1}$ .

between the collimated relativistic outflow from the pulsar and the dense H I cloud. The optical emission associated with RCW 89 can be explained as arising from the ionized outer layers of this high-density material, as first suggested by Manchester (1987).

The total H I mass of the extended filament has been estimated at  $M \sim 4000 M_{\odot}$ , where an appropriate background correction has been applied. An average atomic density  $n \sim 12 \text{ cm}^{-3}$  has been calculated for this elongated H I feature by assuming that the dimension along the line of sight equals the size of the minor axis of the filament. In particular, for the denser concentration of this feature, associated with RCW 89, a total mass  $M \sim 1700 M_{\odot}$  and a volume density  $n \sim 15 \text{ cm}^{-3}$  have been derived (in this case a spherical geometry was assumed for the H I feature).

As other evidence of the interaction of G320.4–1.2 with its surroundings, we have searched for accelerated shocked H I gas all along the northern H I filament, especially in the direction of RCW 89, where the major SNR-ISM interaction occurs. We examined several H I spectra, as well as right ascension versus  $V_{\text{LSR}}$  plots (traced at constant declination), looking for high-velocity features, as observed for example in IC 443 (DeNoyer 1977). Within the moderate angular resolution of the present data, no evidence of accelerated H I gas was found.

We have also investigated the characteristics of the interstellar gas where the southeastern lobe of G320.4–1.2 has expanded. To carry out this calculation we have considered a sample volume in a location relatively free of H I concen-

trations around  $V_{\text{LSR}} \sim -68 \text{ km s}^{-1}$ , the systemic velocity of G320.4–1.2. The obtained volume density is  $n \sim 0.4 \text{ cm}^{-3}$ .

The observed contrast in density between the H I near the northwestern lobe and the ambient H I in the interior of the SNR is consistent with the model of G99 in which the northwestern half of the SNR has encountered the edge of a cavity, while the southeastern half has expanded relatively unimpeded into a lower density environment.

2. *The bright filament perpendicular to the Galactic plane in the interval  $+10 \lesssim V_{\text{LSR}} \lesssim +20 \text{ km s}^{-1}$ .*—Figure 5 displays in detail this H I filament (*thick black contours*), overlaid on radio continuum (*gray scale*) and X-ray (*light gray contours*) emission from the SNR. The cross indicates the position of PSR B1509–58.

From a morphological point of view, there is a striking alignment of this H I filament with both the northwest-southeast axis of the X-ray nebula and the weak radio features extending south of RCW 89. *ROSAT* and *Chandra* data demonstrate that the elongated X-ray nebula represents opposed collimated outflows directed (in projection) along this northwest-southeast axis (Brazier & Becker 1997; Gaensler et al. 2001). G99 argue that the radio emission in this region corresponds to a cylindrical sheath surrounding the pulsar outflow; it has been shown that the magnetic field in the region is well ordered and oriented in a direction parallel to the axis of the proposed outflow (Milne, Caswell, & Haynes 1993; G99). It is thus conceivable that a preexisting column of gas with an orientation similar to that of the out-

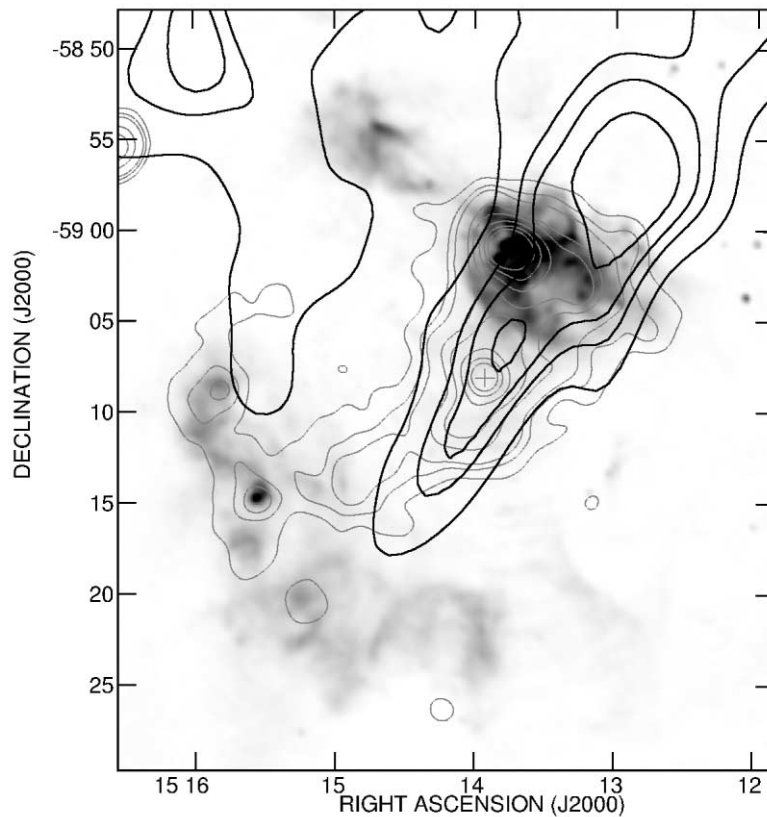


FIG. 5.—Comparison between radio continuum, X-rays, and H I in the velocity range +10 to +20 km s<sup>-1</sup>. X-ray emission from the region (Trussoni et al. 1996) is overlaid in light gray contours. The H I contours are 3, 3.6, 4.2, and 4.5 Jy beam<sup>-1</sup> km s<sup>-1</sup>. The cross indicates the position of the pulsar PSR B1509–58.

flow from the pulsar may have provided the conditions necessary to form a cylinder and thus generate the observed characteristics. For instance, the magnetic field could be frozen to the column of cold H I, thus explaining its order and orientation. This H I feature may suggest an association with G320.4–1.2, based solely on the morphology. However, the large difference between the systemic velocity of the SNR and the H I velocity remains unexplained. For this feature a total H I mass  $M \sim 2700 M_{\odot}$  and an average atomic density  $n \sim 10 \text{ cm}^{-3}$  have been estimated.

#### 4. CONCLUSIONS

We have conducted a study of the distribution and kinematics of the interstellar neutral hydrogen in a field around the bilateral SNR G320.4–1.2. This SNR comprises the bright optical–X-ray–radio nebula RCW 89 and the energetic young pulsar B1509–58.

We find several features in H I that suggest that the radio morphology of G320.4–1.2 is a result of the distribution of the surrounding ISM, combined with the action of the pulsar’s relativistic outflows.

The north-northwest bright radio limb of G320.4–1.2 shows the effects of interaction with an extended H I filament with density of  $\sim 12 \text{ cm}^{-3}$  present at the same velocity as that of the SNR ( $V_{\text{LSR}} \sim -68 \text{ km s}^{-1}$ ). In addition, the interaction of the relativistic outflow from PKS B1509–58 with the denser part of this filament ( $n \sim 15 \text{ cm}^{-3}$ ) may have been responsible for the formation of the bright nebula RCW 89 located on the northwestern extreme of

G320.4–1.2. The opposite radio limb of the SNR apparently expanded into a lower density environment ( $n \sim 0.4 \text{ cm}^{-3}$ ) with little distortion from a semicircular shape.

The nature of barrel-shaped SNRs can be explained by assuming that the SNR expands into a low-density cavity with walls almost parallel and the bright radio limbs originate where the expanding shock encounters the walls (Gaensler 1998). In the case of G320.4–1.2, the present H I study has confirmed the existence of the H I wall associated with the north-northwest lobe. However, the observations are not conclusive with respect to the south-southeast H I counterpart. We have identified H I structures with the location and morphology suggestive of an H I–SNR association in this direction. However, the fact that they are detected near  $V_{\text{LSR}} \sim +3.5 \text{ km s}^{-1}$ , indistinguishable in practice from local gas contribution, makes the association uncertain.

Based on morphological coincidences, we suggest a physical association between the SNR and an elongated H I feature with  $V_{\text{LSR}} \sim +15 \text{ km s}^{-1}$ , oriented perpendicular to the Galactic plane. This H I structure is strikingly aligned with the projected axis inferred for the collimated outflows generated by PSR B1509–58. It is difficult to explain the anomalous kinematical velocity of this feature; we suggest that this gas is indeed at the same distance as G320.4–1.2 but suffers from kinematical distortions. Such perturbations in the velocity field are not unexpected in this region, rich in massive stars with powerful stellar winds that have stirred the interstellar material for thousands of years (Georgelin et al. 1987; Lortet, Georgelin, & Georgelin 1987).



We thank the staff of the ATCA for technical support during the observations, and Naomi McClure-Griffiths for providing us with Parkes data from the Southern Galactic Plane Survey. This research was partially funded through a Cooperative Science Program between CONICET (Argentina) and the National Science Foundation and through CONICET grant 4203/96. B. M. G. acknowledges the support of NASA through Hubble Fellowship grant HST-HF-01107.01-A awarded by the Space Telescope Science Insti-

tute, which is operated by the Association of Universities for Research in Astronomy, Inc., for NASA under contract NAS 5-26555. The Australia Telescope is funded by the Commonwealth of Australia for operation as a National Facility managed by CSIRO. The National Radio Astronomy Observatory is a facility of the National Science Foundation operated under cooperative agreement by Associated Universities, Inc.

## REFERENCES

- Bisnovatyi-Kogan, G. S., Lozinskaya, T. A., & Silich, S. A. 1990, *Ap&SS*, 166, 277
- Brazier, K. T. S., & Becker, W. 1997, *MNRAS*, 284, 335
- Brighenti, F., & D'Ercole, A. 1994, *MNRAS*, 270, 65
- Caswell, J. L., Murray, J. D., Roger, R. S., Cole, D. J., & Cooke, D. J. 1975, *A&A*, 45, 239
- DeNoyer, L. K. 1977, *ApJ*, 212, 416
- Dubner, G. M., Giacani, E. B., Goss, W. M., Moffett, D. A., & Holdaway, M. 1996, *AJ*, 111, 1304
- Dubner, G., Giacani, E., Reynoso, E., Goss, W. M., Roth, M., & Green, A. 1999, *AJ*, 118, 930
- Dubner, G. M., Green, A. J., Goss, W. M., Bock, D. C.-J., & Giacani, E. 1998a, *AJ*, 116, 813
- Dubner, G. M., Holdaway, M., Goss, W. M., & Mirabel, I. F. 1998b, *AJ*, 116, 1842
- Fich, M., Blitz, L., & Stark, A. A. 1989, *ApJ*, 342, 272
- Frazer, R. H., Brooks, J. W., & Whiteoak, J. B. 1992, *J. Electrical Electron. Eng. Australia*, 12, 103
- Fulbright, M. S., & Reynolds, S. P. 1990, *ApJ*, 357, 591
- Gaensler, B. M. 1998, *ApJ*, 493, 781
- Gaensler, B. M., Arons, J., Kaspi, V. M., Pivovarov, M. J., Kawai, N., & Tamura, K. 2001, *ApJ*, submitted
- Gaensler, B. M., Brazier, K. T. S., Manchester, R. N., Johnston, S., & Green, A. J. 1999, *MNRAS*, 305, 724 (G99)
- Georgelin, Y. M., Boulesteix, J., Georgelin, Y. P., Laval, A., & Marcelin, M. 1987, *A&A*, 174, 257
- Giacani, E. B., Dubner, G. M., Green, A. J., Goss, W. M., & Gaensler, B. M. 2000, *AJ*, 119, 281
- Kesteven, M. J., & Caswell, J. L. 1987, *A&A*, 183, 118
- Lortet, M. C., Georgelin, Y. P., & Georgelin, Y. M. 1987, *A&A*, 180, 65
- Manchester, R. N. 1987, *A&A*, 171, 205
- McClure-Griffiths, N. M., Green, A. J., Dickey, J. M., Gaensler, B. M., Green, A. J., Haynes, R. F., & Wieringa, M. H. 2001, *ApJ*, 551, 394
- Milne, D. K., Caswell, J. L., & Haynes, R. F. 1993, *MNRAS*, 264, 853
- Sault, R. J., & Killeen, N. E. B. 1999, *The MIRIAD User's Guide* (Sydney: Australia Telesc. Natl. Facility)
- Sault, R. J., Staveley-Smith, L., & Brouw, W. N. 1996, *A&AS*, 120, 375
- Stanimirović, S. 1999, Ph.D. thesis, Univ. Western Sydney
- Tamura, K., Kawai, N., Yoshida, A., & Brinkmann, W. 1996, *PASJ*, 48, L33
- Trussoni, E., Massaglia, S., Caucino, S., Brinkmann, W., & Aschenbach, B. 1996, *A&A*, 306, 581
- van Langevelde, H. J., & Cotton, W. D. 1990, *A&A*, 239, L5
- Whiteoak, J. B. Z., & Green, A. J. 1996, *A&AS*, 118, 329
- Willingale, R., West, R. G., Pye, J. P., & Stewart, G. C. 1996, *MNRAS*, 278, 749